Int. J. Dev. Biol. 69: 123-131 (2025)
https://doi.org/10.1387/ijdb.240249ai

THE INTERNATIONAL JOURNAL OF DEVELOPMENTAL BIOLOGY
www.intjdevbiol.com

Innervation of the masseter requires Mllt11 (Af1q/Tcf7c) function during trigeminal ganglion development

NICHOLAS W. ZINCK, DANIELLE STANTON-TURCOTTE, EMILY A. WITT, MARLEY BLOMMERS, ANGELO IULIANELLA*

Department of Medical Neuroscience, and Brain Repair Centre, Faculty of Medicine, Dalhousie University, Life Science Research Institute, Halifax, Nova Scotia, Canada

ABSTRACT The development of cranial nerves, including the trigeminal nerve, and the formation of neuromuscular junctions (NMJs) are crucial processes for craniofacial motor function. Mllt11/Af1q/Tcf7c (hereafter Mllt11), a novel type of cytoskeletal-interacting protein, has been implicated in neuronal migration and neuritogenesis during central nervous system development. However, its role in peripheral nerve development and NMJ formation remains poorly understood. This study investigates the function of Mllt11 during trigeminal ganglion development and its impact on motor innervation of the masseter muscle. We report Mllt11 expression in the developing trigeminal ganglia, suggesting a potential role in cranial nerve development. Using a conditional knockout mouse model to delete *Mllt11* in Wnt1-expressing neural crest cells, we assessed trigeminal ganglion development and innervation of the masseter muscle in the jaw. Surprisingly, we found that *Mllt11* loss does not affect the initial formation of the trigeminal ganglion but disrupts its placodal vs. neural crest cellular composition. Furthermore, we showed that conditional inactivation of *Mllt11* using *Wnt1*^{Cre2} led to a reduction of neurofilament density and NMJs within the masseter muscle, along with a reduction of Phox2b^{+} branchiomotor neurons in rhombomere 2, indicating altered trigeminal motor innervation. This was due to the surprising finding that the *Wnt1*$^{Cre2/+}$ mouse driver promoted aberrant recombination and reporter gene expression within branchiomotor neuron pools in rhombomere 2, as well as targeting neural crest cell populations. Our findings show that Mllt11 regulates the cellular composition of the trigeminal ganglion and is essential for proper trigeminal motor innervation in the masseter muscle.

KEYWORDS: Mllt11/Af1q/Tcf7c, trigeminal nerve, masseter, jaw muscles, neuromuscular junction, neural crest cell derivatives

Introduction

The peripheral nervous system comprises the cranial and spinal nerves, which function in relaying sensory and motor signals between the central nervous system and somatic tissues. The cranial peripheral nerves are derived from the neural crest cells (NCCs) and from specialized regional thickenings of the cranial ectoderm called placodes (D'Amico-Martel and Noden, 1983; Hamburger, 1961; Koontz *et al.,* 2023; Trainor, 2014). During cranial nerve neurogenesis, both neural crest cells and ectodermal placode cells delaminate from their respective epithelia, interact, and ultimately lead to the formation of the peripheral nerves (Hamburger, 1961; Kurosaka *et al.,* 2015). While peripheral nerve development has been a subject of study for many decades, the process is not fully understood.

The cranial nerves (CNI-CNXII) are a subset of peripheral nerves originating from the supraspinal elements of the central nervous system. In mice, the cranial nerves emerge at approximately embryonic day (E) 9.5, and axonal projection is apparent by E10.5 (Kurosaka *et al.,* 2015; Sudiwala and Knox, 2019). Each of the twelve cranial nerves provides either sensory, motor, or mixed sensory/motor function to the craniofacial and cervical regions, as well as various abdominothoracic viscera in the case of parasympathetic innervation via the vagus nerve (CNX) (Cordes, 2001). The variety and importance of functions regulated by the cranial nerves are highlighted by the various disorders associated with cranial nerve dysinnervation, collectively known as *cranial nerve dysinnervation disorders*. In the literature, special attention has been paid to disorders characterized by dysinnervation of the oculomotor (CNIII),

***Address correspondence to:** Angelo Iulianella. Department of Medical Neuroscience, and Brain Repair Centre, Faculty of Medicine, Dalhousie University, Life Science Research Institute, Halifax, Nova Scotia, Canada. E-mail: angelo.iulianella@dal.ca | https://orcid.org/0000-0003-0712-4295

Submitted: 18 December, 2024; Accepted: 25 June, 2025; Published online: 1 August, 2025.

ISSN: Online 1696-3547, Print 0214-6282

trochlear (CNIV), trigeminal (CNV), abducens (CNVI) nerves due to their importance in ocular and facial motor function (Kaeser and Brodsky, 2013; Traboulsi, 2004). Multiple genes are implicated in the pathogenesis of these disorders, including tubulin (*Tubb3*), kinesin (*Kif21a*), signal transduction proteins, and various transcription factors (*Sall4, Phox2a*, *Hoxa1*, *Hoxb1*) (Gutowski and Chilton, 2015). A further understanding of cranial nerve development is crucial to understand the pathophysiology of cranial nerve dysinnervation disorders.

The trigeminal ganglion (Vg) is a large sensory and motor nucleus that innervates the vertebrate face and jaw and consists of three main branches, the ophthalmic, maxillary, and mandibular nerves. Their axons originate from principal sensory neurons from within the brain stem, which connect to mesencephalic and spinal tracts (Covell and Noden, 1989). The development of the trigeminal nerve is a long-studied and complex process, with much of the early work utilizing the chicken embryo (Moody and Heaton, 1983a; Moody and Heaton, 1983b; Moody and Heaton, 1983c). Moody and Heaton (Moody and Heaton, 1983a; Moody and Heaton, 1983b) demonstrated that the Vg is required for organization of the trigeminal motor nucleus and subsequent outgrowth of motor axons. Interestingly, when membranes were placed between the trigeminal motor nucleus and the Vg, motor axons would circumvent the obstruction to interact with cell bodies in the Vg (Moody and Heaton, 1983c). In these experiments, only the motor axons that could intercalate with the Vg were able to innervate their motor targets, demonstrating that formation and interactions involving the Vg are required for trigeminal motor development. The branchiomotor neurons that innervate the masseter arise from rhombomere 2 of the hindbrain and chart along the V3 branch of the trigeminal nerve and are involved in jaw elevation and protrusion. These brachiomeric motor pools are specified by the paired homeobox transcription factor Phox2b, which is expressed in ventro-medial regions of the rostral hindbrain (Kang *et al.,* 2007; Pattyn *et al.,* 2000).

Cytoskeletal formation and remodeling are critical processes in both neurogenesis and neuritogenesis (i.e., the formation of axons and dendrites), enabling cell migration, differentiation, and neurite growth (da Silva and Dotti, 2002). We previously characterized Myeloid/lymphoid or mixed-lineage leukemia; translocated to chromosome 11 or ALL1 fused from chromosome 1q or T cell factor 7 cofactor (Mllt11/AF1q/Tcf7c; thereafter referred to as Mllt11) as a vertebrate-specific cytoskeletal-associating protein with restricted expression in the developing central nervous system by E9.5 and in the peripheral ganglia from E10.5 onwards (Yamada *et al.,* 2014). More recently, we showed that Mllt11 is required for neuritogenesis of cortical neurons both *in vitro* and *in vivo*, with *Mllt11* mouse null mutants exhibiting markedly reduced cortical neurite length and complexity, which affected the formation of cortical white matter tracts and commissural projections (Stanton-Turcotte *et al.,* 2022). In the same study, we also showed that *Mllt11* loss-of-function resulted in reduced migration of neurons towards the cortical plate. Mllt11 has also been implicated in cell migration and morphogenesis during retinogenesis. Specifically, knockout of *Mllt11* led to failed migration of retinal ganglion cells and amacrine cells during retinal lamination, and these cells were unable to elongate and assume a bipolar morphology consistent with migrating neuroblasts, and instead adopted a more globular morphology associated with reduced migratory ability (Blommers *et al.,* 2023). While we previously showed that Mllt11 regulates neuronal migration and neuritogenesis in the central nervous system, its role in the peripheral nervous system has yet to be explored. Using a *Wnt1*$^{Cre2/+}$ approach to inactivate a floxed *Mllt11* allele in NCC derivatives, we now report a requirement for *Mllt11* in the formation of the trigeminal nerve, the largest cranial nerve, and innervation of the masseter muscle. That was due, at least in part, to a reduction of Phox2b^{+} branchiomotor neurons in rhombomere 2, which exhibited unexpected *Wnt1*$^{Cre2/+}$ recombination activity in the embryonic hindbrain. Our findings are consistent with a role for Mllt11 in the development of branchiomotor neurons, including neuritogenesis and formation of neuromuscular connections to the muscles of the head.

Results

Previous studies have identified the expression of Mllt11 in the cranial ganglia (Yamada *et al.,* 2014). In order to verify *Mllt11* activity in the developing trigeminal ganglia, we utilized a β-gal knock-in allele for the *Mllt11* locus, as we previously described (Stanton-Turcotte *et al.,* 2022). Visualization of β-gal expression at E12.5 suggests that the *Mllt11* locus is active within the trigeminal ganglion during development (Fig. 1 A,B). We next sought to determine the role of *Mllt11* in the formation of the trigeminal ganglion. To investigate this, we generated *Wnt1*$^{Cre2/+}$; *Mllt11*$^{flox/flox}$; *R26r*$^{TdTomato/+}$ conditional knockout (cKO) embryos that had undergone targeted deletion of *Mllt11* driven by the *Wnt1*^{Cre2} transgenic allele to target NCC derivatives (Dinsmore *et al.,* 2022; Stanton-Turcotte *et al.,* 2022). We focused on the development of the trigeminal ganglion as it is the largest cranial ganglion that is significantly contributed by NCCs (Kurosaka *et al.,* 2015; Moody and Heaton, 1983b).

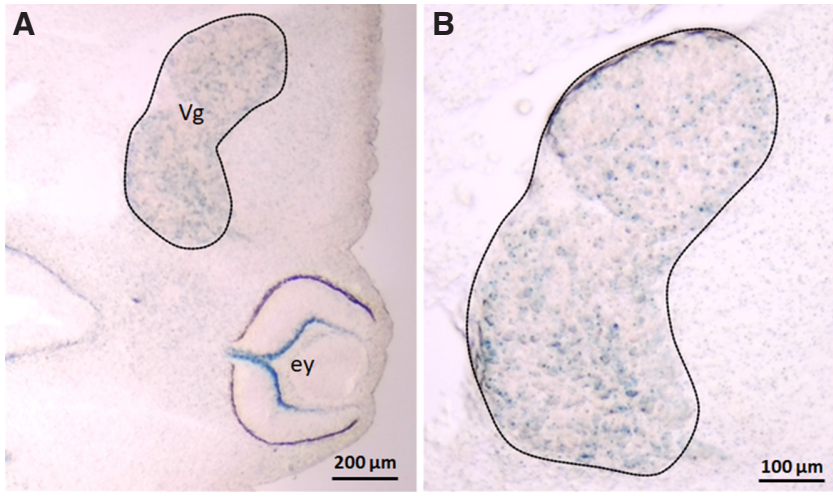

Fig. 1. *Mllt11* is expressed in the trigeminal ganglion. (A)*Mllt11* locus with a β-gal knock-in cassette reveals expression in the trigeminal ganglion (Vg) at E12.5. **(B)** High magnification view of Vg depicted in (A). Blue stain represents X-gal expression resulting from *Mllt11* locus activity. Vg, trigeminal ganglion; ey, eye.

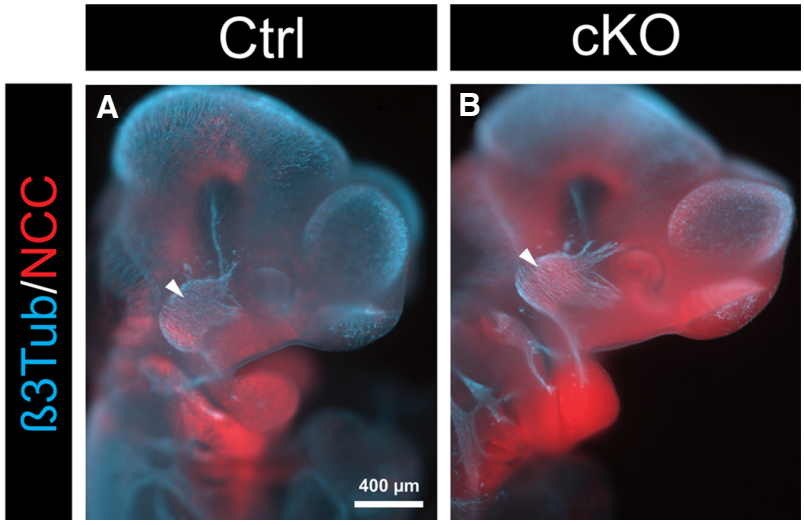

Fig. 2. Normal trigeminal (Vg) nerve morphology in *Mllt11* mutants. (A, B) Whole-mount immunohistochemistry for neuronal-specific βTubulin (β3Tub) at E10.5 illustrating normal Vg cranial nerve morphology in *Mllt11* cKO mutants (B) relative to control wildtype mouse embryos (A, Cntl). Blue, β3Tub; red, *Wnt1*$^{Cre2/+}$; *Rosa26r*$^{tdTomato/+}$ fate map; lateral view. Arrowhead indicates trigeminal ganglion.

***Mllt11* is not required for the formation of the trigeminal ganglia**

We first confirmed *Wnt1*$^{Cre2/+}$ transgene activity in the NCC neurogenic derivatives of the embryonic head, using *Cre*$^{+}$ males to generate NCC-specific targeting, as recommended previously (Dinsmore *et al.*, 2022), by profiling Ai9 *TdTomato* reporter activity. The resulting Tomato^{+} signal identified NCC fate-mapped populations through the craniofacial region, including the trigeminal nerve and its branches, which were visualized by β-tubulin III (β3Tub) whole mount immunostaining at E10.5. We observed no difference in overall trigeminal ganglion morphology (Fig. 2 A,B), suggesting that the initial formation of the structure is unaffected by *Mllt11* loss. We next examined whether *Mllt11* loss affected the cellular composition of the ganglia in the *Wnt1*$^{Cre2/+}$-driven *Mllt11* cKO mice using markers for cells arising from the neural crest (Sox10) vs. embryonic ectodermal placodes (Isl1/2) (Figs. 3 and 4, respectively). At E12.5, there was no statistically significant difference in the mean number of cells within the ganglia (Fig. 3 A,D,G; Table 1; p=0.739, T-test). Additionally, there was no statistically significant difference in the proportion of *Wnt1*$^{Cre2/+}$-fate labeled Tomato^{+} NCCs (Fig. 3 B,E,H; Table 1; p=0.184, T-test) or Sox10^{+} cells (Fig. 3 C,F,I; Table 1; p=0.215, T-test) relative to DAPI^{+} cells populating the trigeminal ganglion. Interestingly, *Mllt11* cKO mice displayed a high degree of variation in total cell density (Fig. 3G), as well as the proportion of Tomato^{+} NCCs (Wnt1^{+}) and Sox10^{+} cells, relative to controls (Fig. 3 H,I). Moreover, *Mllt11* cKOs displayed a significant reduction in the ratio of Wnt1^{+} NCCs to Sox10^{+} cells within the trigeminal ganglion, compared to controls (Fig. 3J; Table 1; p=0.013, T-test). We next probed for alterations

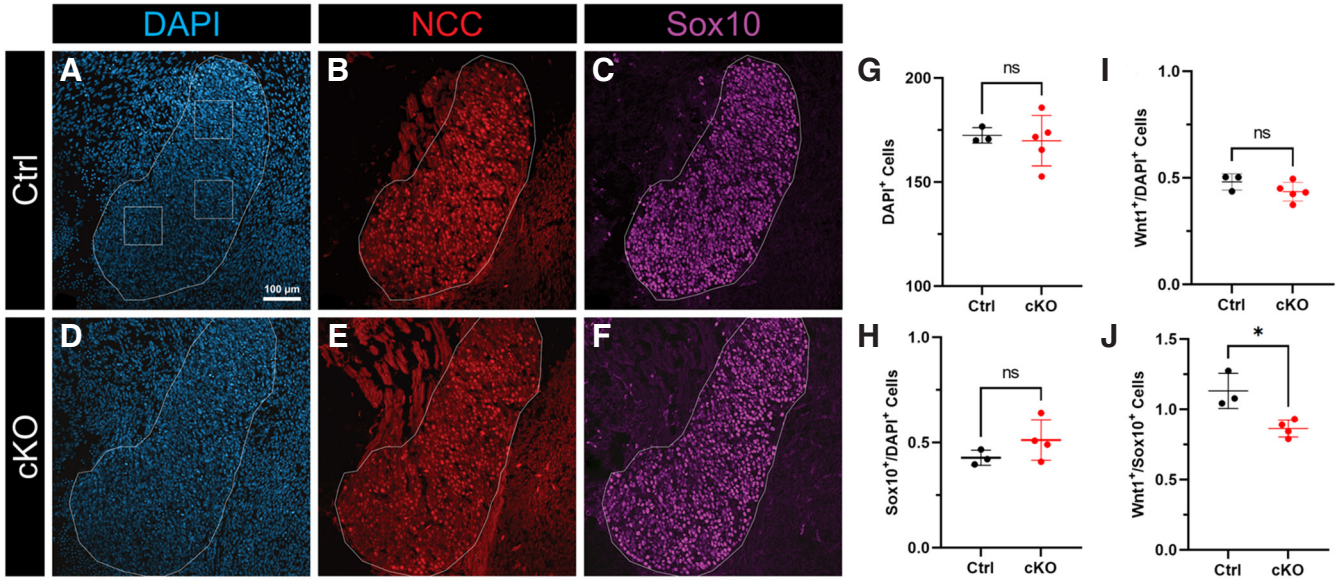

Fig. 3. Reduced numbers of NCC-derived Sox10^{+} cells in *Mllt11* cKO mutants. (A-F) Control and *Mllt11* cKO E12.5 trigeminal ganglia positive for DAPI (A-D), NCCs (*Wnt1*$^{Cre2/+}$; *Rosa26r*$^{tdTomato/+}$; B, E), and Sox10 (C, F) in transverse sections. Ganglia are outlined in white. Boxes represent example ROIs for cell-count sampling. **(G-J)** plots comparing the total cell density (G), proportion of NCC (H) and Sox10^{+} (I) cells, and the ratio of NCCs^{+} to Sox10^{+} cells (J) in the trigeminal ganglia between control (black) and *Mllt11* cKO embryos (red). Error bars indicate standard deviation; ns, not statistically significant; * p < 0.05. Abbreviations: NCC, neural crest cells; ROI, region of interest.

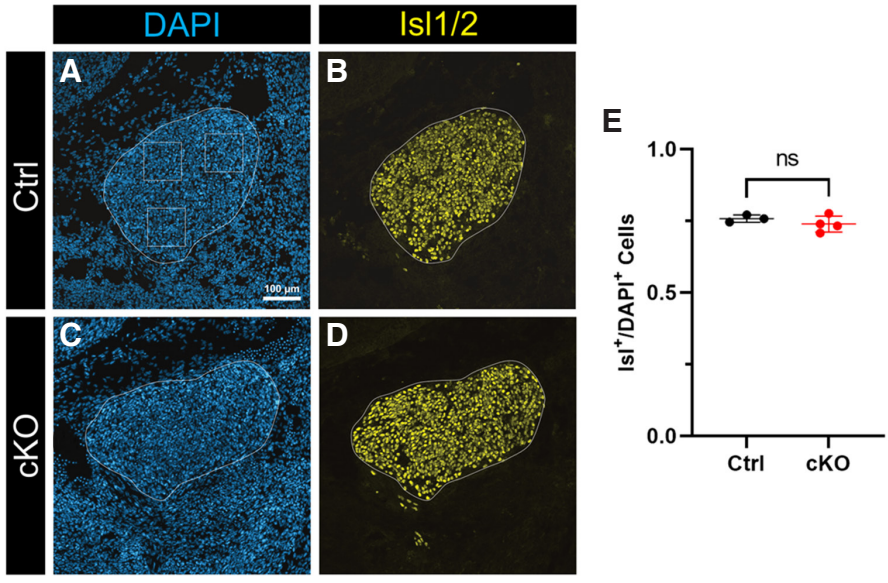

Fig. 4. Placode-originating cells are unaffected in *Mllt11* cKO mutants. (A-D) Control and cKO E12.5 Vg stained with DAPI (A, C) and anti-Isl1/2 (B, D). Ganglia are outlined in white. Boxes represent example ROIs for cell-count sampling. **(E)** plot comparing ratio of Isl1/2$^+$ and DAPI$^+$ cells between controls (black) and *Mllt11* cKO (red) placodes. Error bars indicate standard deviation; ns, not statistically significant. Abbreviations: ROI, regions of interest; Vg, trigeminal ganglia.

in placodal populations of the trigeminal ganglion by comparing the number of Isl1/2-expressing cells between control (Fig. 4 A,B) vs. *Mllt11* cKO mutants (Fig. 4 C,D), but found no difference in the number of Isl1/2$^+$ cells (Fig. 4E; Table 1; p=0.329, n=4, T-test). This suggested that *Wnt1*$^{Cre2/+}$-driven *Mllt11* cKOs specifically affected NCC-derived populations of the ganglion, such as Sox10$^+$ glial cells, and not placodal cells, which are instead derived from ectoderm.

Given that *Mllt11* loss subtly affected the NCC-derived cell numbers in the trigeminal ganglion, we evaluated if this was due to enhanced cell death by staining for Cleaved Caspase-3 (CC3) (Porter and Janicke, 1999). CC3$^+$ cells were detected in E12.5 control (Fig. 5 A-C) and *Mllt11* cKO (Fig. 5 D-F) trigeminal ganglia, but we found no evidence of enhanced apoptosis in cKO ganglia (Fig. 5G; Table 1; p=0.263, T-test).

Mllt11 cKO in NCCs disrupts trigeminal motor innervation of the masseter

The Vg is required for trigeminal motor innervation via interactions between motor axons and cell bodies within the Vg (Moody and Heaton, 1983a; Moody and Heaton, 1983b; Moody and Heaton, 1983c). As no major difference in trigeminal ganglion development was obvious at E12.5, we reasoned that *Wnt-1*$^{Cre2/+}$- mediated ablation of *Mllt11* in NCC derivatives, or possibly

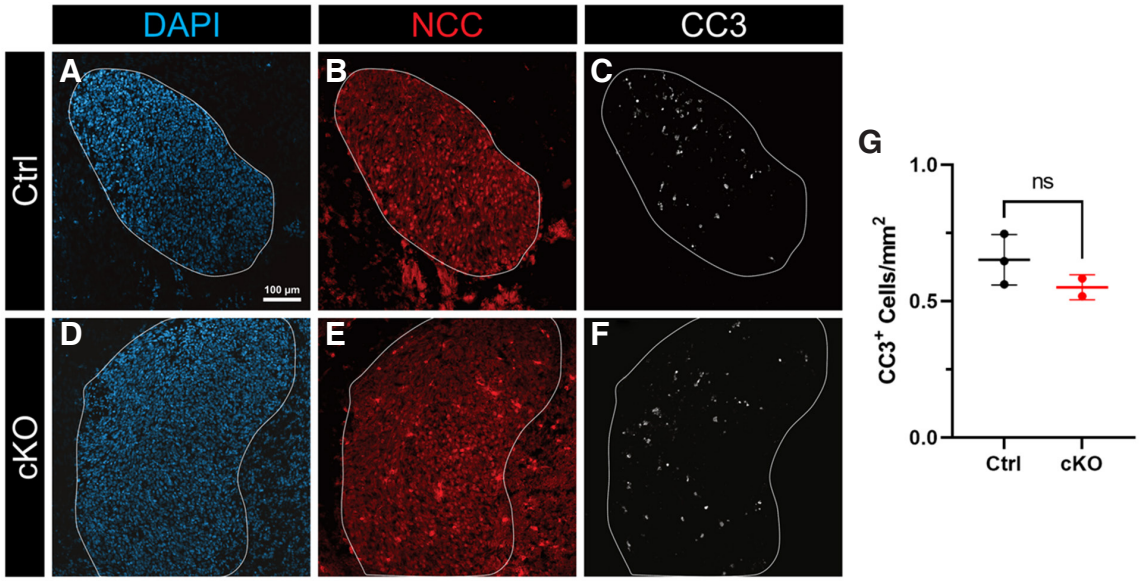

Fig. 5. Trigeminal ganglion composition differences in *Mllt11* cKO mutants is not due to cell death. (A-F) Control (A-C) and *Mllt11* cKO (D-F) E12.5 trigeminal ganglia stained with DAPI (A, D), NCC-fate mapped cells (red, B, E), and Cleaved Caspase 3 (CC3; white, C, F) in transverse sections. Ganglia are outlined in white. **(G)** plot comparing density of CC3$^+$ cells in the E12.5 trigeminal ganglia in control (black)vs. *Mllt11* cKO (red) embryos. Error bars indicate standard deviation; ns, not statistically significant.

branchiomotor neurons (see below), may lead to defects in the ganglion that may impair its role in supporting trigeminal motor innervation. We focused on trigeminal motor innervation and examined the presence of nerve fibers and neuromuscular junctions (NMJs) in the masseter muscle. We used neurofilament (NF) immunostaining along with neuromuscular endplate labeling with fluorescent bungarotoxin (BTX) staining, which identifies nicotinic acetylcholine (nAChRs) receptors on muscle fibers. Interestingly, we observed a high degree of variation in NF density in the masseter of E18.5 *Mllt11* cKOs compared to controls (Fig. 6 B,E,H,J,M; Table 2; p=0.066, T-test), with the majority of individuals exhibiting reduced NF$^+$ fiber staining in the masseter relative to controls (Fig. 6M). In contrast to the disruption in NF bundle density, we did not observe a difference in the density of BTX$^+$ staining of NMJs between control and cKO mice (Fig. 6 C,F,H,J,N; Table 2; p=0.120, T-test). Under higher magnification, we confirmed a striking reduction in the number of NMJs (NF$^+$/BTX$^+$) in E18.5 *Mllt11* cKO mouse masseters compared to controls (Fig. 6 H,J,O; Table 2; p=0.034, T-test). Together, these results demonstrate that inactivation of *Mllt11* in NCCs and their neurogenic derivatives leads to disruptions in trigeminal nerve motor innervation of the masseter.

We next focused on the development of branchiomotor pools that send axons along the V3 branch of the Vg to innervate the masseter. To do this, we examined the distribution of neurons expressing the paired box homeodomain transcription factor Phox2b, which is required for the specification of brachiomeric-targeting motor neurons from the hindbrain, but not required for innervating somatic muscles (Pattyn *et al.*, 2000). *Wnt1*$^{Cre2/+}$*; R26r*$^{TdTomato/TdTomato}$ E11.5 embryos showed extensive labeling of NCC derivatives, but surprisingly also showed reporter activity in the rostral hindbrain, in rhombomere 2 (Fig. 7A). We therefore examined rhombomere 2 motor neurons by staining for Phox2 and NF in longitudinal sections across the hindbrain of E11.5 embryos (section angle indicated in Fig. 7A). In *Wnt1*$^{Cre2/+}$*; R26r*$^{TdTomato/TdTomato}$ control embryos, Phox2$^+$/ NF$^+$ double positive cells were distributed in medial pools next to the mantle zone (mz, Fig. 7 B-D). Confirming the whole mount analysis, we observed Tomato$^+$ recombination activity within the mz and Phox2b$^+$ branchiomotor neurons in rhombomere 2. These are not NCC-derived tissues and reflect aberrant *Wnt1*$^{Cre2/+}$ activity within the ventromedial region of the rostral hindbrain. Interestingly, in *Wnt1*$^{Cre2/+}$*; Mllt-11*$^{flox/flox}$*; R26r*$^{TdTomato/TdTomato}$ cKOs we noted a decrease

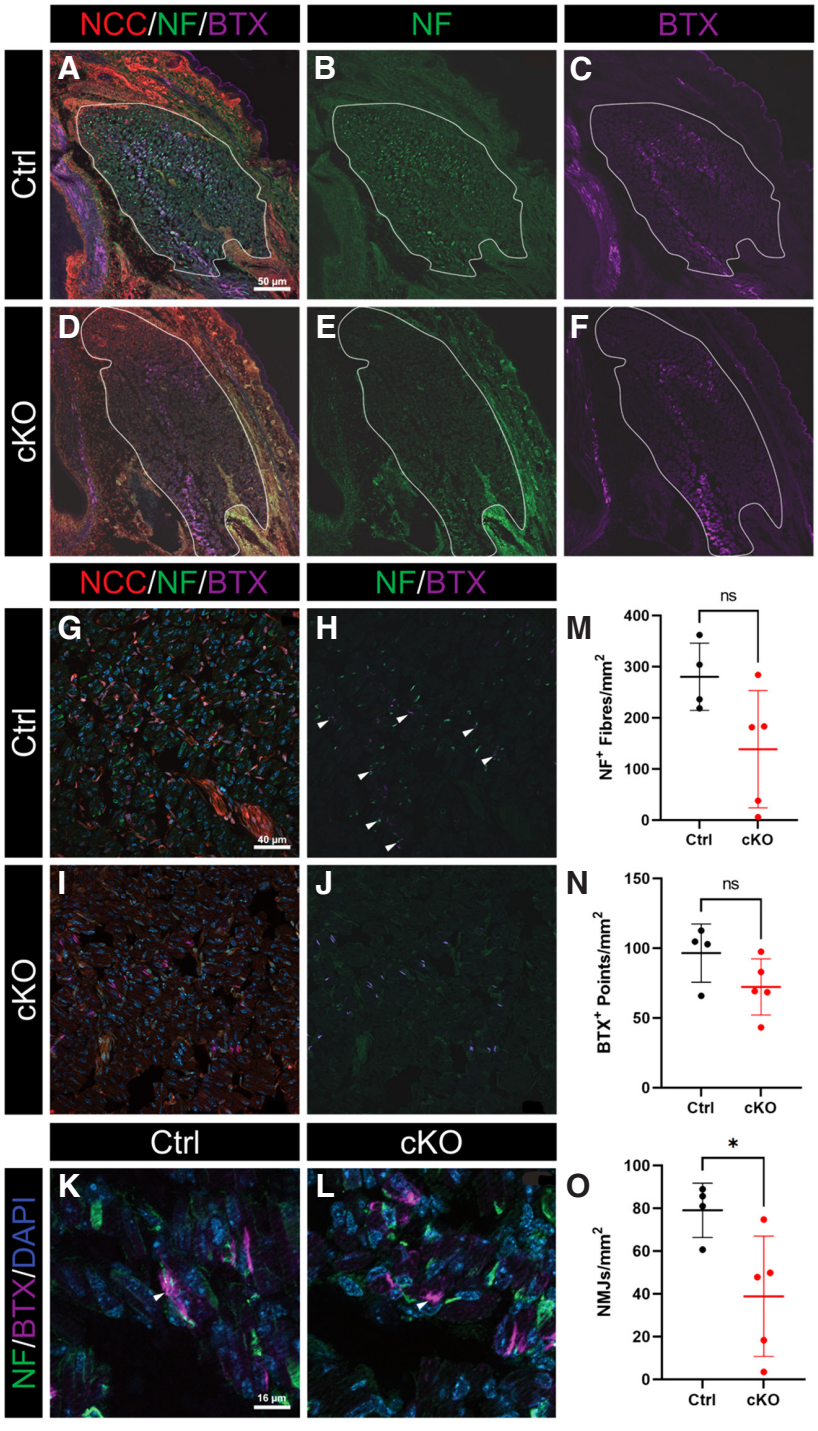

Fig. 6. Masseter muscle innervation is disrupted in *Mllt11* cKO fetuses. (A-F) Transverse sections of control (Ctrl, A-C) and *Mllt11* cKO (D-F) mouse E18.5 masseter muscles in displaying NCC-fate mapped cells (red; A, B), neurofilament (NF) identifying nerve fibers (A-E), and BTX stain identifying clustered nicotinic acetylcholine receptors (nAChR) characteristic of NMJs (purple; A, C, D, F). (A-F) Muscles are outlined in white. **(G-J)** Higher magnification views of the masseter NMJs consisting of NF$^+$ (green) and BTX$^+$ (purple) revealed close contact of nerve fibers and muscle in control (G, H; arrowheads in H), but *Mllt11* cKO masseter NMJ lacked co-staining of intramuscular BTX$^+$/NF$^+$ signal (J). **(K)** Representative image of control (K) NMJs displaying interdigitation of NF$^+$ fibers in BTX$^+$ NMJs. **(L)** *Mllt11* cKOs displayed disrupted NMJs, with a failure of NF$^+$ fibers to enwrap BTX$^+$ NMJs. **(M-O)** Plots comparing density of NF$^+$ fibers (L), BTX$^+$ points (M), and NMJs (N), normalized over muscle area, between control (black) and *Mllt11* cKO (red) mice, which showed significantly reduced NMJs. Error bars indicate standard deviation; ns, no statistically significant difference; *, $p < 0.05$. Abbreviations: NMJ, neuromuscular junction, BTX, bungarotoxin toxin.

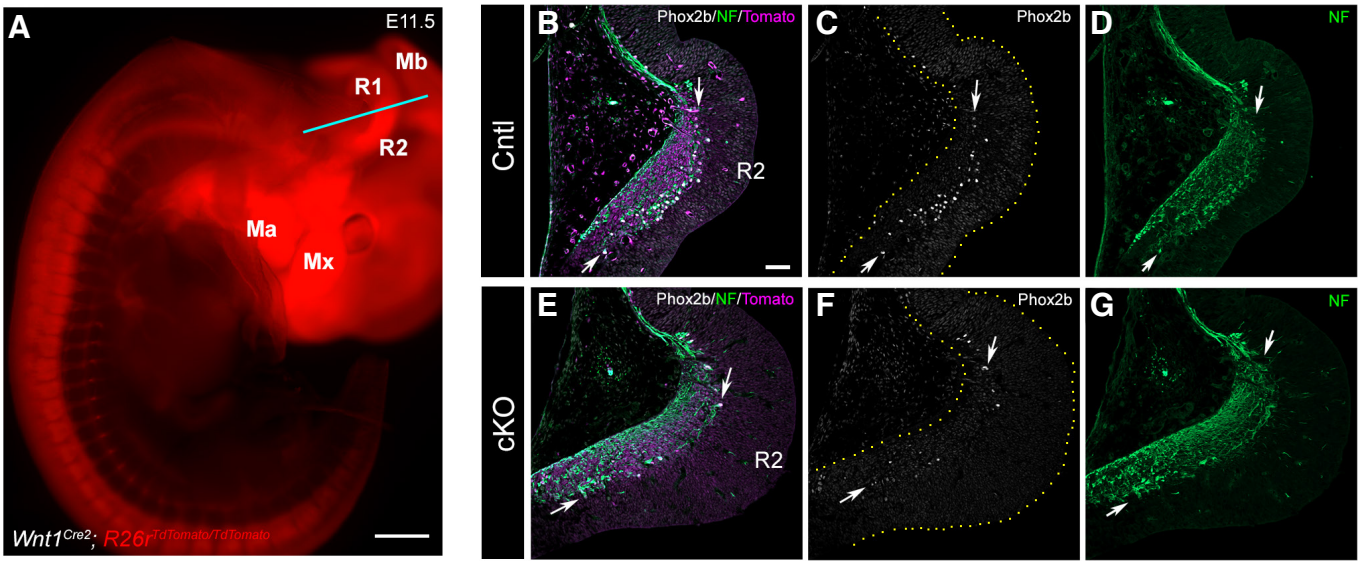

Fig. 7. *Wnt1*$^{Cre2/+}$ activity in rhombomere 2 led to reduced Phox2b^{+} branchiomotor neurons in *Mllt11* cKO mutants. (A) Whole mount of E11.5 *Wnt1*$^{Cre2/+}$; *R26r*$^{TdTomato/TdTomato}$ control embryo. Tomato^{+} expression reflects recombination activity in NCC-derived tissues, including peripheral nerves. Aberrant Tomato^{+} activity was noted in R2. Line indicates longitudinal sectioning plane at the level of R2 depicted in B-G. **(B-D)** Merge of immunostaining of Phox2b (white, C), NF (green, D), and Tomato expression (fuchsia, B) in *Wnt1*$^{Cre2/+}$; *R26r*$^{TdTomato/TdTomato}$ control (Cntl) R2 region. Arrows in indicate Phox2b^{+} branchiomotor pool adjacent NF^{+} mz. (B) Tomato^{+} activity reflecting *Wnt1*$^{Cre2/+}$-mediated recombination in mz and adjacent Phox2b^{+} cells (arrows). **(E-G)** Merge of immunostaining of Phox2b (white, F), NF (green, G), and Tomato expression (fuchsia, E) in *Wnt1*$^{Cre2/+}$; *Mllt11*$^{flox/flox}$; *R26r*$^{TdTomato/TdTomato}$ conditional knockout (cKO) R2 region. (F) Arrows indicate reduced Phox2b^{+} branchiomotor neurons in cKO. Scale bar: A, 500μm; B, 50μm. Abbreviations: Ma, mandible; Mb, midbrain; Mx, maxillary; mz, mantle zone, NF, neurofilament; R1, rhombomere 1; R2, rhombomere.

in Phox2b^{+}/NF^{+} branchiomotor pools clustered medially from the mz (arrows, Fig. 7 E-G; N=4 cKOs, N=3 controls). This region overlapped with Tomato^{+} activity (Fig. 7E), demonstrating that *Mllt11* loss in differentiating Phox2b^{+} cells within rhombomere 2 using the *Wnt1*$^{Cre2/+}$driver led to reductions of motor neurons that target the masseter.

TABLE 1

COMPARISONS OF TRIGEMINAL GANGLION CELLULAR COMPOSITION AT E12.5

Comparison	Control Mean ± SD; n	cKO Mean ± SD; n	P-value
DAPI+ cells	172.5 ± 3.688; 3	169.9 ± 12.11; 5	0.739
NCC/ DAPI+ cells	0.481 ± 0.038; 3	0.435 ± 0.044; 5	0.184
Sox10+/ DAPI+ cells	0.428 ± 0.036; 3	0.512 ± 0.096; 4	0.215
NCC/ Sox10+ cells	1.132 ± 0.125; 3	0.864 ± 0.060; 4	0.013
Isl1/2+/DAPI+ cells	0.758 ± 0.013; 3	0.739 ± 0.028; 4	0.329
CC3+ cells/mm2	0.652 ± 0.093; 3	0.552 ± 0.046; 2	0.263

SD, standard deviation. NCCs were fate labeled with Tomato+. P-value derived from T-test.

TABLE 2

COMPARISON OF NMJ INNERVATION OF THE MASSETER MUSCLE AT E18.5

Comparison	Control Mean ± SD; n	cKO Mean ± SD; n	P-value
NF+ fibers/mm2	280.5 ± 65.8; 4	138.8 ± 114.8; 5	0.066
BTX+ points/mm2	96.6 ± 20.88; 4	72.34 ± 20.10; 5	0.120
NMJs/mm2	79.11 ± 12.71; 4	38.89 ± 28.13; 5	0.034

SD, standard deviation. P-value derived from T-test.

Discussion

The aim of this study was to determine if the novel cytoskeletal-interacting protein Mllt11 plays a role in the formation of the trigeminal ganglion. Previous studies have demonstrated its requirement for neurogenic processes in different systems throughout the mammalian nervous system, including migration and neuritogenesis in the lamination of the neocortex, retina, and cerebellum (Blommers *et al.,* 2023; Blommers *et al.,* 2024; Stanton-Turcotte *et al.,* 2022). Here we show that Mllt11 is required for the proper innervation of the masseter. Using *Wnt1*^{Cre2} to ablate *Mllt11* within NCC-derived cranial nerves, we demonstrated that Mllt11 plays a role in maintaining the composition of the trigeminal ganglia and the innervation of a trigeminal motor target, the masseter. Because Mllt11 regulates neuritogenesis in the CNS, it is possible that its NCC-specific knockout leads to microarchitectural changes in the Vg, disrupting interactions with trigeminal motor axons. Surprisingly, during this study, we noted that *Wnt1*^{Cre2} activity was present in rhombomere 2, specifically encompassing most of the branchiomotor pool that innervates the masseter. This is not a NCC-derived population and instead represents aberrant Cre activity within the CNS, and when mated to *Mllt11*$^{flox/flox}$ mice, resulted in a reduction of Phox2b^{+} branchiomotor neurons. Our findings raise concerns about using the *Wnt1*$^{Cre2/+}$ mouse driver allele to evaluate gene function in sensory vs motor development in the craniofacial region.

In the trigeminal ganglion at E12.5, fate-mapped NCCs (Tomato+ cells) and Sox10^{+} cells represent a mix of both neurons and glia (Schwann cells), as both populations arise from the neural crest (Koontz *et al.,* 2023; Le Douarin and Smith, 1988; Méndez-Maldonado *et al.,* 2020). We observed a modest reduction in NCC-derived

Sox10$^+$, but not placodal (Isl1/2$^+$), upon *Wnt1*$^{Cre2/+}$-mediated *Mllt11* ablation. However, *Mllt11* loss in Wnt1$^+$ cells did not appear to overtly affect NCC migration, as evidenced by largely normal patterns of NCC fate-mapped Tomato$^+$ cells populating trigeminal ganglia. Nor was the reduction of Sox10$^+$ due to enhanced cell death. We, therefore, wondered if the deletion of *Mllt11* in NCC derivatives had any secondary effects on the trigeminal system, specifically on its interaction with trigeminal motor inputs to the masseter. We found that *Mllt11* loss in peripheral ganglia resulted in reduced motor innervation of the masseter, as evidenced by the reduction of NF density and NF$^+$/BTX$^+$ (i.e. NMJs) in the muscle. NMJs are critical sites for communication between motor neurons and muscle fibers, and their proper assembly is essential for muscle contraction and motor control.

Kummer *et al.,* (Kummer *et al.,* 2004) demonstrated the cell-autonomous ability of skeletal muscle cells to form the post-synaptic motor assembly *in-vitro* without a neuronal presence or signal. This is consistent with our *in vivo* observations of the maintenance of nAChRs in masseters of *Wnt1*$^{Cre/+}$*; Mllt11*$^{flox/flox}$ mutants despite the loss of invading neurites. The main role of the masseter is mastication; however, it plays a minor role in facial expression and speech, by stabilizing the mandible, in humans (Kent, 2004). In mice, the role of the masseter is limited more to mastication and biting, providing the main muscle mass for these functions. Future research into the role of *Mllt11* in craniofacial nervous system development should examine the behavioral manifestations of the knockout in post-natal mice.

Despite the reduction in innervation in the *Mllt11* mutants, we did not observe any change in the density of BTX-rich regions, signifying that they maintained post-synaptic assembly of the nAChR-dense apparatus. This is not surprising given that *Mllt11* expression is restricted to developing neurons (Yamada *et al.,* 2014) and our genetic strategy using the *Wnt1*$^{Cre2/+}$ driver intended to ablate *Mllt11* primarily in peripheral neurons. However, while previous reports did not indicate *Wnt1*^{Cre} activity in motor nuclei of the rostral hindbrain (Chen *et al.,* 2017), a recent report demonstrated that the rederived *Wnt1*$^{Cre2/+}$ mouse allele does indeed show aberrant recombination in the ventral neural tube (Gandhi *et al.,* 2024). Indeed, our investigations revealed unexpected *Wnt1*$^{Cre2/+}$*;R26r*$^{TdTomato/TdTomato}$ recombination activity in the Phox2b$^+$ branchiomotor pools in rhombomere 2 and the adjacent mantle zone at E11.5. This was associated with reductions in Phox2b$^+$ rostral hindbrain motor neurons in *Mllt11* cKOs, likely contributing to reduced NMJ formation in the masseter at late fetal stages.

Concerning possible molecular targets of Mllt11 action in nerve development, we previously identified α/β Tubulins, Actin, and atypical Myosins as potential Mllt11-interaction targets in the fetal brain (Stanton-Turcotte *et al.,* 2022). The role of the cytoskeleton in NCC development is supported by work in chicken embryos showing that β3Tub is expressed in pre-neuronal cells of the neural plate and dorsal neural tube, that is, the pre-migratory neural crest (Chacon and Rogers, 2019). Interestingly, this expression coincides with the upregulation of NCC-specific markers such as *Sox10*. In contrast, *Mllt11* does not appear to be expressed in the pre-migratory or migratory NCCs. Instead, it is expressed later in differentiated neurons throughout the central and peripheral nervous systems, co-expressing with robust β3Tub levels (Yamada *et al.,* 2014). It is currently unclear whether Mllt11 promotes cytoskeletal dynamics in filopodia and growth cones to promote migration and axonogenesis, but its cytoskeletal association and neuritogenic phenotype in the cranial ganglia suggest that it may promote the formation of stabilized structures in the axon shaft (da Silva and Dotti, 2002; Kapitein and Hoogenraad, 2015). Similarly, in the CNS, *Mllt11* is required for the formation of long-range axonal connections across the corpus callosum and the formation of complex dendritic arborizations in cortical pyramidal neurons (Stanton-Turcotte *et al.,* 2022). In addition, *Mllt11* promotes the migration of immature neurons in the cortex and retina, reflecting its expression in nascent neurons or neuroblasts (Blommers *et al.,* 2023; Stanton-Turcotte *et al.,* 2022). Given the restricted expression of *Mllt11* in developing cranial ganglia and CNS neurons, but not in migrating crest cells, we reasoned that *Mllt11* loss most acutely affected outgrowth of peripherally targeting axons in the craniofacial region; a process that depends on cytoskeletal dynamics. Our findings are consistent with Mllt11 being a microtubule-interacting protein functioning to stabilize the cytoskeleton (Stanton-Turcotte *et al.,* 2022).

However, in our investigations, we discovered that the widely used *Wnt1*$^{Cre2/+}$ allele for targeting NCC populations is also active in the rostral hindbrain mantle zone and at least some branchiomotor neurons in rhombomere 2. This confounded our interpretation of the tissue of origin of jaw muscle innervation defects we observed in the *Mllt11* cKOs. Namely, we observed reductions in the Phox2b$^+$ branchiomotor neuron pool in rhombomere 2, likely accounting at least in part for the reduced innervation of masseter. Furthermore, the neuritogenetic defects in *Mllt11* cKO peripheral neurons also contributed to reduced neuromuscular connectivity in the masseter. Reduced branchiomotor development in rhombomere 2 of *Wnt1*$^{Cre2/+}$ driven *Mllt11* cKOs may also explain the subtle disruptions in Vg cellular composition, as interactions between the Vg and V motor axons growing from the brain stem may affect the differentiation of cranial ganglia (Moody and Heaton, 1983a; Moody and Heaton, 1983b). While the *Wnt1*$^{Cre2/+}$*; Mllt11* cKO phenotype was variable, in the most striking examples of masseter dysinnervation we observed a near total absence of NF$^+$ fibers in the periphery near the muscle target. Future research should expand the analysis presented in this study to examine any possible effects on the innervation of other craniofacial muscles and cutaneous sensory structures.

Conclusions

This study demonstrates that the novel protein Mllt11 plays a role in the formation of the trigeminal ganglion and branchiomotor innervation of one of its target muscles, the masseter. We showed that *Mllt11* deficiency using the *Wnt1*$^{Cre2/+}$ mouse driver allele led to alterations in the normal balance of cell types in the ganglion, reduced Phox2b$^+$ branchiomotor pools in rhombomere 2, and disrupted the motor innervation from the trigeminal ganglion. The most likely explanation for the phenotype is a combination of reduced branchiomotor neurons and altered neurite outgrowth of cranial nerves following *Mllt11* ablation, leading to reduced interactions between the trigeminal ganglion and trigeminal motor fibers, and failed axonal endplate integration in the masseter muscle. Cranial nerves, including the trigeminal nerve, play crucial roles in functions such as facial motor control and sensation. As such, these findings have important implications for our understanding of cranial nerve development and motor function. Our study provides a foundation for future research on cranial ganglion development and the investigation of mechanisms regulating peripheral nerve innervation.

Materials and Methods

Animals

All experiments were done according to approved protocols from the IACUC at Dalhousie University. *Mllt11*$^{flox/flox}$*; Rosa26r*$^{TdTomato/TdTomato}$ (or *R26r*$^{TdTomato/TdTomato}$; Ai9; Jackson Laboratory strain#00709) reporter mice were generated and genotyped as previously described (Stanton-Turcotte *et al.,* 2022). NCC-specific ablation of *Mllt11* was accomplished by mating female *Wnt1*$^{Cre2/+}$ driver mice (B6. Cg-E2f1Tg(Wnt1-cre)2Sor/J; Jackson laboratory strain#022501) with male *Mllt11*$^{flox/+}$*; R26r*$^{TdTomato/TdTomato}$ to generate conditional knockouts (cKOs) used in this study. To generate neural crest cell-specific ablation of *Mllt11*, the *Wnt1*$^{Cre2/+}$ allele was derived maternally, as previously reported (Dinsmore *et al.,* 2022). Confirmation of trigeminal ganglion *Mllt11* expression was done using the targeted pre-floxed *Mllt11* allele, which houses a β-galactosidase (β-gal) cassette (*Mllt11*$^{tm1a(KOMP)Mbp}$) (Stanton-Turcotte *et al.,* 2022).

Histology

Embryos were dissected from maternal decidua and either whole embryos (E11.5 and E12.5) or heads (E18.5) were fixed in 4% paraformaldehyde in phosphate buffer for four hours, cryoprotected in sucrose gradient, and embedded in optimum cutting temperature (OCT) compound (Tissue-Tek, Torrance, CA). Embedded samples were stored at -80°C until sectioning. Samples were cryosectioned at 20 µm transversely (for the cranial nerve analysis) or 14 µm longitudinally (for the hindbrain analysis) and stored at -20°C until stained. β-gal staining was performed with the *Mllt11*$^{tm1a(KOMP)Mbp}$ targeted allele (Stanton-Turcotte *et al.,* 2022), using serial incubations with warmed β-Galactosidase Stain Base Solution A and then Solution B, according to manufacturer's instructions (Millipore, Burlington, MA), and staining with X-gal solution (Novagen, Madison, WI).

Immunohistochemistry

Frozen sections were permeabilized by incubating in 0.1% Triton/Phosphate Buffered Saline with 0.1% Triton X-100 (PBT) and incubated in 3% normal donkey serum (NDS)/3% bovine serum albumin (BSA)/0.1% PBT for 1h at room temperature. The sections were then incubated with primary antibodies overnight at 4°C. Primary antibodies utilized include rabbit anti-Sox10 (1/100, Abcam), mouse anti-Isl1/2 (1/25, DSHB), mouse anti-Neurofilament 2H3 (1/200, DSHB), rabbit anti-Phox2b (1/350, Invitrogen/ThermoFisher), and rabbit anti-Cleaved Caspase-3 (1:500, Cell Signaling Technology). α-bungarotoxin (BTX) conjugated with Alexa Fluor 647 (1:500, Invitrogen) was used to visualize nicotinic acetylcholine receptor densities. Species-specific Alexa Fluor 488-, 568-, and 647-conjugated secondary antibodies were used to detect primary antibodies (1:1500, Invitrogen). Following antibody staining, nuclei were counterstained with DAPI (4',6-diamidino-2-phenylindole; 0.6mg/mL, Sigma). Following washes, slides were mounted (DakoCytomation fluorescent mounting medium) and stored at 4°C until imaging.

For whole-mount immunostaining, embryos were dissected in Phosphate Buffered Saline (PBS), selected for tdTomato+ reporter (*R26r*$^{TdTomato/TdTomato}$) expression in *Wnt1*$^{Cre2/+}$-fate mapped neural crest cell derivatives, fixed with 4% paraformaldehyde/PBS pH 7.4 for 4-5 hours at 4°C, rocking. Then embryos were rinsed in PBT and blocked in 3% Donkey Serum/1% Bovine Serum Albumin/PBT for 2-24 hours at 4°C. After genotyping embryos, controls (*Wnt*$^{Cre2/+}$*; Mllt11*$^{Flox/+}$*; R26r*$^{TdTomato/TdTomato}$) were pooled separately from *Mllt11* cKO mutants (*Wnt1*$^{Cre2/+}$*; Mllt11*$^{flox/flox}$*; R26r*$^{TdTomato/TdTomato}$) and incubated with mouse anti-β3 Tubulin (TuJ1, 1:1000, MilliporeSigma) antibodies overnight at 4°C, rocking. The following day, embryos were rinsed extensively in PBT and incubated with donkey anti-mouse Alexa Fluor 488 secondary antibodies (1:1000, Invitrogen) overnight at 4°C, rocking. The following day, embryos were rinsed in PBT, counterstained with DAPI, and cleared in glycerol/PBS buffer.

Microscopy and Imaging

Microscopy was performed using a Zeiss AxioObserver fluorescence microscope equipped with an Apotome 2, 10x and 20x objectives, and a Hamamatsu Orca Flash v4.0 digital camera. For whole-mount immunostaining, microscopy was performed using a Zeiss V16 Zoomscope equipped with an Axiocam 506 digital camera. Images were captured using Zen software (Zeiss, Baden-Württemberg, Germany), and montages were assembled using Photoshop (Adobe, San Jose, CA) and Affinity Photo 2 (Serif, Nottinghamshire, UK).

Image sampling, quantification, and analysis

Cell counts were performed at E12.5 for DAPI, Sox10, Isl1/2$^+$ cells, and *Wnt1*^{Cre}*; tdTomato*$^+$ fate-mapped NCCs. Three regions of interest (ROI) 100 x 100 µm in size were randomly placed over images of immunostained sections of trigeminal ganglia and the number of cells within each ROI was counted using ImageJ (Fiji). For each individual animal, this was performed on three serial sections of the same ganglion. Cell counts were normalized to the number of DAPI$^+$ cells in the same ROI (e.g., *Wnt1*$^{Cre2/+}$; Tomato+/DAPI$^+$ cells) and averaged for each individual animal. These values are represented by data points in Figs. 2, 3, 4.

Cell counts were conducted at E18.5 within a ROI comprising the total area of the masseter muscle due to the non-uniform nature of nerve distribution within the masseter. For each individual animal, this was performed on three serial sections of the same ganglion. Cell counts were normalized to the total area of the ROI and averaged for each individual animal. These values are represented by data points in Figs. 6 and 7. An identical method utilizing normalization to a ROI encompassing the cross-sectional area of the masseter was used for analysis of the CC3 signal in the E12.5 cell death assay (Fig. 5).

Acknowledgments

We gratefully acknowledge funding from the National Science and Engineering Research Council of Canada (RGPIN 03925-20), the Dalhousie University Faculty of Medicine Gladys Osman Estate, and the Killam Foundation for fellowship support to EW. We thank Sarah Whitehead for assistance with animal husbandry and Dr. Victor Rafuse for BTX reagents.

Author contributions

NWZ sectioned, immunostained, analyzed the data, generated figures, and wrote the first draft. MB and AI assisted with microscopy. DST and EAW helped with tissue preparation, mouse embryo generation, expression analysis, genotyping, and figures. AI supervised the project, obtained funding, conducted whole mount and section immunostaining and microscopy, edited figures and manuscript.

Funding

National Science and Engineering Research Council of Canada (RGPIN 03925-20).

References

BLOMMERS M., STANTON-TURCOTTE D., IULIANELLA A. (2023). Retinal neuroblast migration and ganglion cell layer organization require the cytoskeletal-interacting protein Mllt11. *Developmental Dynamics* 252: 305-319. https://doi.org/10.1002/dvdy.540

BLOMMERS M., STANTON-TURCOTTE D., WITT E. A., HEIDARI M., IULIANELLA A. (2024). Cerebellar granule cell migration and folia development require Mllt11/Af1q/Tcf7c. *Developmental Neurobiology* 84: 74-92. https://doi.org/10.1002/dneu.22936

CHACON J., ROGERS C. D. (2019). Early expression of Tubulin Beta-III in avian cranial neural crest cells. *Gene Expression Patterns* 34: 119067. https://doi.org/10.1016/j.gep.2019.119067

CHEN G., ISHAN M., YANG J., KISHIGAMI S., FUKUDA T., SCOTT G., RAY M. K., SUN C., CHEN S.Y., KOMATSU Y., MISHINA Y., LIU H.X. (2017). S pecific and spatial labeling of P0-Cre versus Wnt1-Cre in cranial neural crest in early mouse embryos. *genesis* 55: 10.1002/dvg.23034. https://doi.org/10.1002/dvg.23034

CORDES S. P. (2001). Molecular genetics of cranial nerve development in mouse. *Nature Reviews Neuroscience* 2: 611-623. https://doi.org/10.1038/35090039

COVELL D. A., NODEN D. M. (1989). Embryonic development of the chick primary trigeminal sensory-motor complex. *Journal of Comparative Neurology* 286: 488-503. https://doi.org/10.1002/cne.902860407

D'AMICO-MARTEL A., NODEN D. M. (1983). Contributions of placodal and neural crest cells to avian cranial peripheral ganglia. *American Journal of Anatomy* 166: 445-468. https://doi.org/10.1002/aja.1001660406

DA SILVA J. S., DOTTI C. G. (2002). Breaking the neuronal sphere: regulation of the actin cytoskeleton in neuritogenesis. *Nature Reviews Neuroscience* 3: 694-704. https://doi.org/10.1038/nrn918

DINSMORE C. J., KE C.Y., SORIANO P. (2022). The Wnt1-Cre2 transgene is active in the male germline. *genesis* 60: e23468. https://doi.org/10.1002/dvg.23468

GANDHI S., DU E.J., PANGILINAN E.S., HARLAND R.M. (2024). The Wnt1-Cre2 transgene causes aberrant recombination in non-neural crest cell types. *bioRxiv* Preprint: 2024.11.06.622365. https://doi.org/10.1101/2024.11.06.622365

GUTOWSKI N. J., CHILTON J. K. (2015). The congenital cranial dysinnervation disorders. *Archives of Disease in Childhood* 100: 678-681. https://doi.org/10.1136/archdischild-2014-307035

HAMBURGER V. (1961). Experimental analysis of the dual origin of the trigeminal ganglion in the chick embryo. *Journal of Experimental Zoology* 148: 91-123. https://doi.org/10.1002/jez.1401480202

KAESER P.F., BRODSKY M. C. (2013). Fourth Cranial Nerve Palsy and Brown Syndrome: Two Interrelated Congenital Cranial Dysinnervation Disorders?. *Current Neurology and Neuroscience Reports* 13: 352. https://doi.org/10.1007/s11910-013-0352-5

KANG B.J., CHANG D.A., MACKAY D.D., WEST G.H., MOREIRA T.S., TAKAKURA A.C., GWILT J.M., GUYENET P.G., STORNETTA R.L. (2007). Central nervous system distribution of the transcription factor Phox2b in the adult rat. *Journal of Comparative Neurology* 503: 627-641. https://doi.org/10.1002/cne.21409

KAPITEIN L. C., HOOGENRAAD C. C. (2015). Building the Neuronal Microtubule Cytoskeleton. *Neuron* 87: 492-506. https://doi.org/10.1016/j.neuron.2015.05.046

KENT R. D. (2004). The uniqueness of speech among motor systems. *Clinical Linguistics & Phonetics* 18: 495-505. https://doi.org/10.1080/02699200410001703600

KOONTZ A., URRUTIA H. A., BRONNER M. E. (2023). Making a head: Neural crest and ectodermal placodes in cranial sensory development. *Seminars in Cell & Developmental Biology* 138: 15-27. https://doi.org/10.1016/j.semcdb.2022.06.009

KUMMER T. T., MISGELD T., LICHTMAN J. W., SANES J. R. (2004). Nerve-independent formation of a topologically complex postsynaptic apparatus. *The Journal of Cell Biology* 164: 1077-1087. https://doi.org/10.1083/jcb.200401115

KUROSAKA H., TRAINOR P. A., LEROUX-BERGER M., IULIANELLA A. (2015). Cranial Nerve Development Requires Co-Ordinated Shh and Canonical Wnt Signaling. *PLoS One* 10: e0120821. https://doi.org/10.1371/journal.pone.0120821

LE DOUARIN N. M., SMITH J. (1988). Development of the Peripheral Nervous System from the Neural Crest. *Annual Review of Cell Biology* 4: 375-404. https://doi.org/10.1146/annurev.cb.04.110188.002111

MÉNDEZ-MALDONADO K., VEGA-LÓPEZ G. A., AYBAR M. J., VELASCO I. (2020). Neurogenesis From Neural Crest Cells: Molecular Mechanisms in the Formation of Cranial Nerves and Ganglia. *Frontiers in Cell and Developmental Biology* 8: 635. https://doi.org/10.3389/fcell.2020.00635

MOODY S. A., HEATON M. B. (1983a). Developmental relationships between trigeminal ganglia and trigeminal motoneurons in chick embryos. I. Ganglion development is necessary for motoneuron migration. *Journal of Comparative Neurology* 213: 327-343. https://doi.org/10.1002/cne.902130308

MOODY S. A., HEATON M. B. (1983b). Developmental relationships between trigeminal ganglia and trigeminal motoneurons in chick embryos. II. Ganglion axon ingrowth guides motoneuron migration. *Journal of Comparative Neurology* 213: 344-349. https://doi.org/10.1002/cne.902130309

MOODY S. A., HEATON M. B. (1983c). Developmental relationships between trigeminal ganglia and trigeminal motoneurons in chick embryos. III. Ganglion perikarya direct motor axon growth in the periphery. *Journal of Comparative Neurology* 213: 350-364. https://doi.org/10.1002/cne.902130310

PATTYN A., HIRSCH M.R., GORIDIS C., BRUNET J.F. (2000). Control of hindbrain motor neuron differentiation by the homeobox gene Phox2b. *Development* 127: 1349-1358. https://doi.org/10.1242/dev.127.7.1349

PORTER A. G., JÄNICKE R. U. (1999). Emerging roles of caspase-3 in apoptosis. *Cell Death & Differentiation* 6: 99-104. https://doi.org/10.1038/sj.cdd.4400476

STANTON-TURCOTTE D., HSU K., MOORE S. A., YAMADA M., FAWCETT J. P., IULIANELLA A. (2022). Mllt11 Regulates Migration and Neurite Outgrowth of Cortical Projection Neurons during Development. *The Journal of Neuroscience* 42: 3931-3948. https://doi.org/10.1523/JNEUROSCI.0124-22.2022

SUDIWALA S., KNOX S. M. (2019). The emerging role of cranial nerves in shaping craniofacial development. *genesis* 57: e23282. https://doi.org/10.1002/dvg.23282

TRABOULSI E. I. (2004). Congenital abnormalities of cranial nerve development: overview, molecular mechanisms, and further evidence of heterogeneity and complexity of syndromes with congenital limitation of eye movements. *Trans Am Ophthalmol Soc* 102: 373-389.

TRAINOR P.A. (2014). Neural Crest Cells: Evolution, Development and Disease. Elsevier/Academic Press, Amsterdam. pp. 488. https://doi.org/10.1016/C2012-0-00698-9

YAMADA M., CLARK J., IULIANELLA A. (2014). MLLT11/AF1q is differentially expressed in maturing neurons during development. *Gene Expression Patterns* 15: 80-87. https://doi.org/10.1016/j.gep.2014.05.001